ADVANCED FUNCTIONAL MATERIALS
www.afm-journal.de

Stretchable, Transparent, and Thermally Stable Triboelectric Nanogenerators Based on Solvent-Free Ion-Conducting Elastomer Electrodes

Panpan Zhang, Yanghui Chen, Zi Hao Guo, Wenbin Guo, Xiong Pu, and Zhong Lin Wang**

The development of stretchable/soft electronics requires power sources that can match their stretchability. In this study, a highly stretchable, transparent, and environmentally stable triboelectric nanogenerator with ionic conductor electrodes (iTENG) is reported. The ion-conducting elastomer (ICE) electrode, together with a dielectric elastomer electrification layer, allows the ICE-iTENG to achieve a stretchability of 1036% and transmittance of 91.5%. Most importantly, the ICE is liquid solvent-free and thermally stable up to 335 °C, avoiding the dehydration-induced performance degradation of commonly used hydrogels. The ICE-iTENG shows no decrease in electrical output even after storing at 100 °C for 15 h. Biomechanical motion energies are demonstrated to be harvested by the ICE-iTENG for powering wearable electronics intermittently without extra power sources. An ICE-iTENG-based pressure sensor is also developed with sensitivity up to 2.87 kPa^{-1}. The stretchable ICE-iTENG overcomes the strain-induced performance degradation using percolated electrical conductors and liquid evaporation-induced degradation using ion-conducting hydrogels/ionogels, suggesting great promising applications in soft/stretchable electronics under a relatively wider temperature range.

1. Introduction

The rapid development of flexible/stretchable electronics has been hindered by one challenge that most state-of-the-art power devices can hardly match the flexibility, stretchability or multifunctionality of the electronics.[1,2] For example, high stretchability, self-healing capability, or transparency has been realized in many reported electronic skins integrated with multifunctional smart sensors, but the research on compatible energy devices still falls behind.[3–6] Triboelectric nanogenerators (TENGs), which combine triboelectrifcation and electrostatic induction,[3,4] have attracted significant attentions as promising next-generation mechanical energy-harvesting devices due to a high degree of freedom for material selection, a variety of operating sources, a high power-to-weight ratio, and various device structures.[7–13] Several stretchable TENGs have been recently reported by using conductive polymer composites as the electrode, which are realized by mixing conductive materials (carbon nanotubes, graphene, carbon paste, silver nanowires, etc.) into elastomer substrates.[14–20] Nevertheless, the stretchability is limited by the fact that the percolated networks of conductive fillers are broken at large strain.[21] Alternatively, TENGs with ultrahigh stretchability have been reported by using ionic conductors of hydrogels or ionogels.[22–34] Hydrogels are composed of hydrophilic polymer networks swollen with water or ionic aqueous solution, which can be stretchable, biocompatible and transparent.[35–37] However, these devices suffer from poor environmental stability because the ionic conductivity and stretchability of hydrogels or ionogels can be severely deteriorated due to the dehydration or evaporation of liquid solvent.[38–41]

Dr. P. Zhang, Y. Chen, Z. H. Guo, W. Guo, Prof. X. Pu, Prof. Z. L. Wang
CAS Center for Excellence in Nanoscience
Beijing Key Laboratory of Micro-Nano Energy and Sensor
Beijing Institute of Nanoenergy and Nanosystems
Chinese Academy of Sciences
Beijing 100083, China
E-mail: puxiong@binn.cas.cn
Y. Chen, Z. H. Guo, W. Guo, Prof. X. Pu, Prof. Z. L. Wang
School of Nanoscience and Technology
University of Chinese Academy of Sciences
Beijing 100049, China
The ORCID identification number(s) for the author(s) of this article can be found under https://doi.org/10.1002/adfm.201909252.
Prof. X. Pu, Prof. Z. L. Wang
Center on Nanoenergy Research
School of Chemistry and Chemical Engineering
School of Physical Science and Technology
Guangxi University
Nanning 530004, China
Prof. Z. L. Wang
School of Materials Science and Engineering
Georgia Institute of Technology
Atlanta, GA 30332-0245, USA
E-mail: zlwang@gatech.edu

DOI: 10.1002/adfm.201909252

Therefore, an ideal stretchable TENG would utilize both elastomers for electrification materials and electrodes. The elastomer electrode is better to be ionic conductive and free of liquid-phase materials, so the high stretchability and environmental stability can be simultaneously achieved. Solvent-free ion conductive polyelectrolytes [poly(ethylene oxide(PEO), poly(propylene oxide)PPO, polysiloxane (PSI), etc.] have been widely reported for applications in all-solid-state energy storage devices.[42,43] Solvent-free polyelectrolytes are synthesized by salt-in-polymer strategy, achieving conductivity by ionic transportation through polymer chains.[44] Since the there is no liquid solvent, it is quite stable in air, showing neither weight loss nor the decay of its conductivity and mechanical properties. Nevertheless, the stretchability for most solid-state polyelectrolyte is limited, and the report of stretchable ion-conducting elastomers (ICEs) is rare.[45]

Here, we report an ionic triboelectric nanogenerator (iTENG) that enables both biomechanical energy harvesting and touch sensing by using dielectric elastomer as the electrification layer and ion-conductive elastomer as the electrode. Ultrahigh stretchability (ultimate strain ε of 1036%) and high transparency (up to 91.5%) are achieved simultaneously. The soft skin-like nanogenerator is capable of outputting an open-circuit voltage of up to 95 V and an instantaneous areal power density of 55.9 mW m^{-2}. More importantly, the dehydration limitation of previously reported hydrogel is eliminated. The ICE is thermally stable until 335 °C, and the ICE-based iTENG (ICE-iTENG) shows no degradation in output performances even after kept at 100 °C for 15 h. Furthermore, the ICE-iTENG-based sensor, with triangular pyramid surfaces as the electrification layer, can sense pressure of as low as 0.4 kPa. The current study presents an energy harvester and touch sensor that is super-stretchable, biocompatible, transparent, and environmentally stable, suggesting potential applications in smart artificial skins, soft robots, functional displays, and wearable electronics even under relatively high temperature.

2. Results and Discussion

2.1. Basic Properties of ICEs

ICEs were fabricated by a photopolymerization process. Butyl acrylate (BA) monomer was initiated with an ultraviolet (UV) light through free radical polymerization and poly-ethyleneglycol diacrylate (PEGDA) was used as the crosslinker to form elastomer. At the same time, lithium bis(trifluoromethane sulfonimide) (LiTFSI) was used as the electrolyte salt. **Figure 1**a shows the molecular structure of electrolyte salt, monomer, crosslinker, and photo-initiator, respectively. Figure 1b shows the proposed ion transport mechanism within the ICEs matrix. Lithium ions are coordinated by the ether oxygen atoms from the segmental ICEs chain through the complexation by organic carbonates.[43] With the processes of breaking/forming lithium–oxygen (Li—O) bonds, ion transport occurs by intrachain or interchain hooping within the ICEs chains. Accompanied by the gradual replacement of the ligands for the solvation of Li^+, the continuous segmental rearrangement can result in a

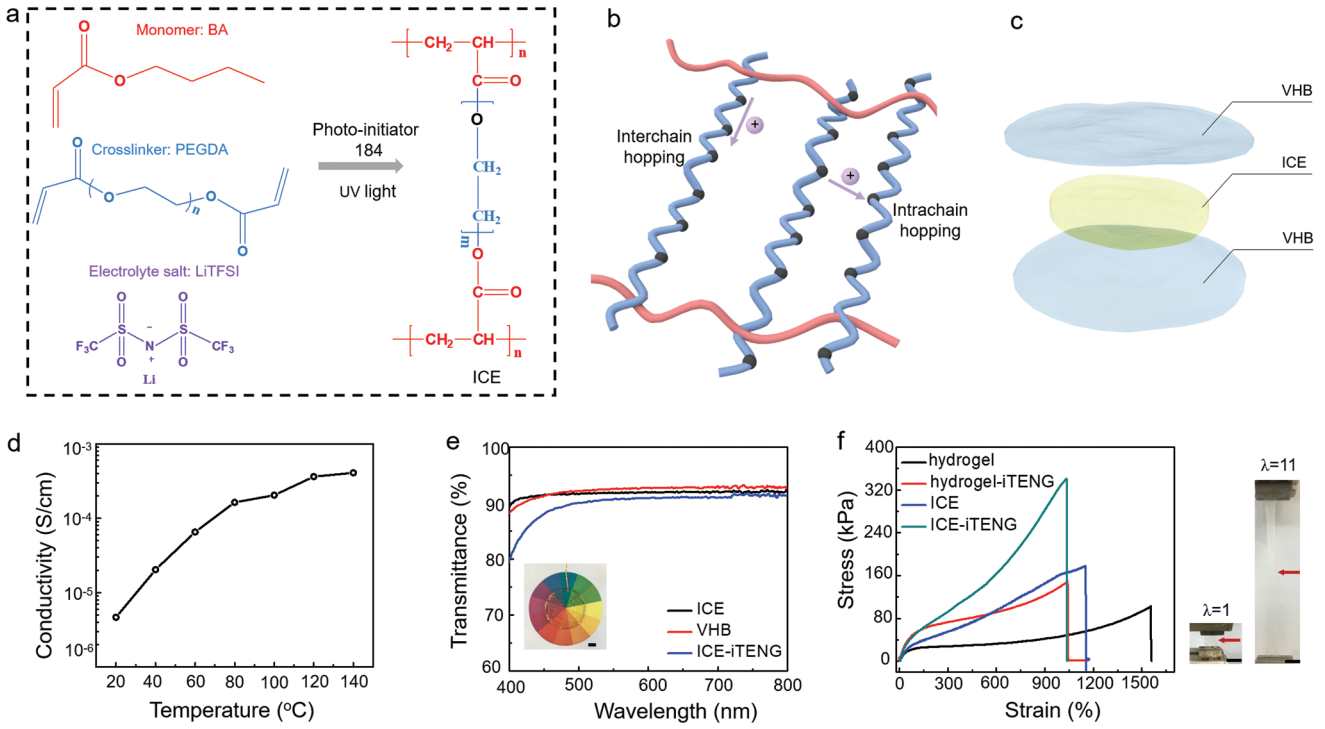

Figure 1. Properties of ICEs. a) Molecular structures of ICE precursors and the polymerized ICE. b) Mechanism of ion transport in ICEs. c) Scheme of the ICE-iTENG with sandwich structure. d) The ionic conductivity of the ICE versus testing temperature. e) Transmittance in the visible range of ICE, VHB elastomer, and the ICE-iTENG. The inset is a photo of the ICE-iTENG (scale bar: 1 cm). f) Stress–strain curves of the ICE, and ICE-iTENG. The photos are the ICE-iTENG (indicated by arrows) at initial state (stretch $\lambda = 1$) and stretched state ($\lambda = 11$ or strain $\varepsilon = 1000\%$) (scale bar: 1 cm).

long-range transport of lithium ions. The electrical properties for ICEs were measured by an alternating-current impedance spectroscopy. Sample was sandwiched between two 304 stainless steel electrodes with diameter of 150 mm, and the thickness of the sample is around 0.6 mm. Similar to liquid electrolytes and gel electrolytes, ICEs showed frequency-dependent impedance. The bulk resistance of ICEs from the Nyquist plot of impedance spectrum was measured. The conductivity was calculated by the equation $\sigma = L/SR$, where L corresponded to the thickness of ICEs, S corresponded to the effective area, and R corresponded to the bulk resistance. The conductivity of ICEs was calculated to be 4.7×10^{-6} S cm^{-1} at 20 °C. ICEs exhibited higher conductivity with increasing the temperature, as shown in Figure 1d. The conductivity of ICEs was 4.1×10^{-4} S cm^{-1} at 140 °C. It was due to the fact that the movement of polymer chains became stronger at higher temperature. So the ion transport through intrachain or interchain hoping within the ICEs chains became easier, resulting in a higher conductivity.

2.2. Properties of ICE-iTENG

The single-electrode-mode iTENG typically has a sandwich structure, as shown in Figure 1c. The ionic electrode was sealed between two 3M VHB 9469 (VHB) films, and a Cu wire was connected to the electrode. Other than using ICE electrode, an iTENG with polyacrylamide (PAAm) hydrogel electrode was also prepared for comparison. The two different iTENGs were denoted as ICE-iTENG and hydrogel-iTENG, respectively. The final devices can be in any shapes and are all elastomers based. The transmittance of ICEs was measured and the results were shown in Figure 1e. The inset image in Figure 1e shows a highly transparent circular ICE-iTENG. A 1-mm-thick ICE showed a transmittance of 92.4% in the visible light wavelength range (400–800 nm), and the corresponding ICE-iTENG showed a transmittance of 91.5%. The literature reported the transmittance of a 2-mm-thick PAAm hydrogel was 98% and the transmittance of the corresponding iTENG was 95% at the same wavelength.[46,47] The transmittance of ICE was almost comparable with the hydrogel. Since the final devices are all elastomer-based, the ICE-iTENG should be stretchable as well, which is confirmed by the images in Figure 1f. The mechanical properties of ICEs and ICE-iTENG were measured (Figure 1f). The ICEs reached a strain to fracture of around 1175%, and the stress at break is around 180 kPa, which is about two times of that of hydrogel; while, the ICE-iTENG ruptures at a stress of 340 kPa and a strain to fracture of 1036%. The stretchability of hydrogel-iTENG and ICE-iTENG is almost same. However, the ultimate stress for ICE-iTENG is two times higher than that of hydrogel-iTENG.

Usually, a TENG operates in one of the four types of working modes, that is, contact separation, sliding, freestanding, and single electrode modes. If the ICEs are connected to the ground through an external load, the ICE-iTENG can work in the single-electrode mode (**Figure 2**a). When a dielectric material contacts with the insulating elastomer of the iTENG, electrification occurs at the interface because of their differences in work functions. Same amount of charges with opposite polarities generate at the surfaces of the dielectric material and the elastomer (Figure 2a, i), respectively. At this moment, the electrical potential difference between the two surfaces is almost zero. When the dielectric material is moving away from the elastomer of the iTENG, the static charges at the surface of the elastomer will induce the movement of the ions within the ICE to balance the static charges, forming a layer of excessive ions at the interface of ICE (Figure 2a, ii). Meanwhile, the electrical double layer formed at the metal/ICEs interface will be polarized, forming the same amount of charges with opposite polarities at the interface between ICE and metal. To achieve this double layer, electrons flow from the metal wires to the ground through the external circuits until all the static charges in the insulating elastomer film are screened (Figure 2a, iii). When the dielectric material is approaching back to the elastomer, the whole process will be reversed and an electron flux with the opposite direction will transfer from the ground to the metal/ICEs interface through the external load (Figure 2a, iv). When the contact-separation movement between the dielectric material and the ICE-iTENG is repeated, an alternative current will be generated.

The output of the ICE-iTENG was measured with a commercial Nylon film to carry out the contact-separation movement (area, 3×3 cm^2). The peak open-circuit voltage V_{OC} and the peak short-circuit charge Q_{SC} are about 90 V and 30 nC as shown in Figure 2b, respectively. Under short-circuit conditions, an alternative current was measured with a peak value of ≈1.25 μA (see Figure 2b). By varying the external resistance, the maximum output areal power density was measured to be 55.9 mW m^{-2} at a matched resistance of ≈200 MΩ as shown in Figure 2c.

Since the ICE-iTENG shows the high stretchability, the energy harvesting properties of the iTENG at stretched states were further studied. Figure 2d shows an ICE-iTENG (area, 3 cm × 2.5 cm) was uniaxially stretched for different stretches. The corresponding electrical outputs for a latex film doing the contact-separation motion are shown in Figure 2e. The corresponding Q_{SC} at stretched states are shown in Figure S1 in the Supporting Information. During the measurement, the shape and size of the latex film were kept to be close to the ICE-iTENG at each stretched state. At initial state without strain ($\lambda = 1$), the V_{OC} of the iTENG is 60 V. When the ICE-iTENG is stretched at $\lambda = 3$ and 8, the V_{OC} is improved to ≈112 and ≈163 V, respectively. The Q_{SC} at stretched states also increased. These results are similar with the previously reports.[46,48]

The V_{OC} and Q_{SC} have a relationship of $Q_{SC} = V_{OC}\ C_o$, in which C_o is the capacitance of the iTENG. The V_{OC} and Q_{SC} can be estimated as:[49,50]

$$V_{OC} = -\sigma A/2C_o \quad (1)$$

$$Q_{SC} = -\sigma A/2 \quad (2)$$

where σ donates the density of electrostatic charges formed at the surface of the elastomer, and A donates the contacting area between the dielectric material and the elastomer of the iTENG. At stretched state, the surface area of the elastomer increased, resulting in a bigger contacting area for the electrification. Based on Equations (1) and (2), the V_{OC} and Q_{SC} increase due to the bigger contacting area A at stretched state. In our measurement, the area of the iTENG is almost doubled when the iTENG is stretched to $\lambda = 3$. So the V_{OC} of the iTENG is improved around 1 times from ≈60 to ≈112 V after being stretched for $\lambda = 3$.

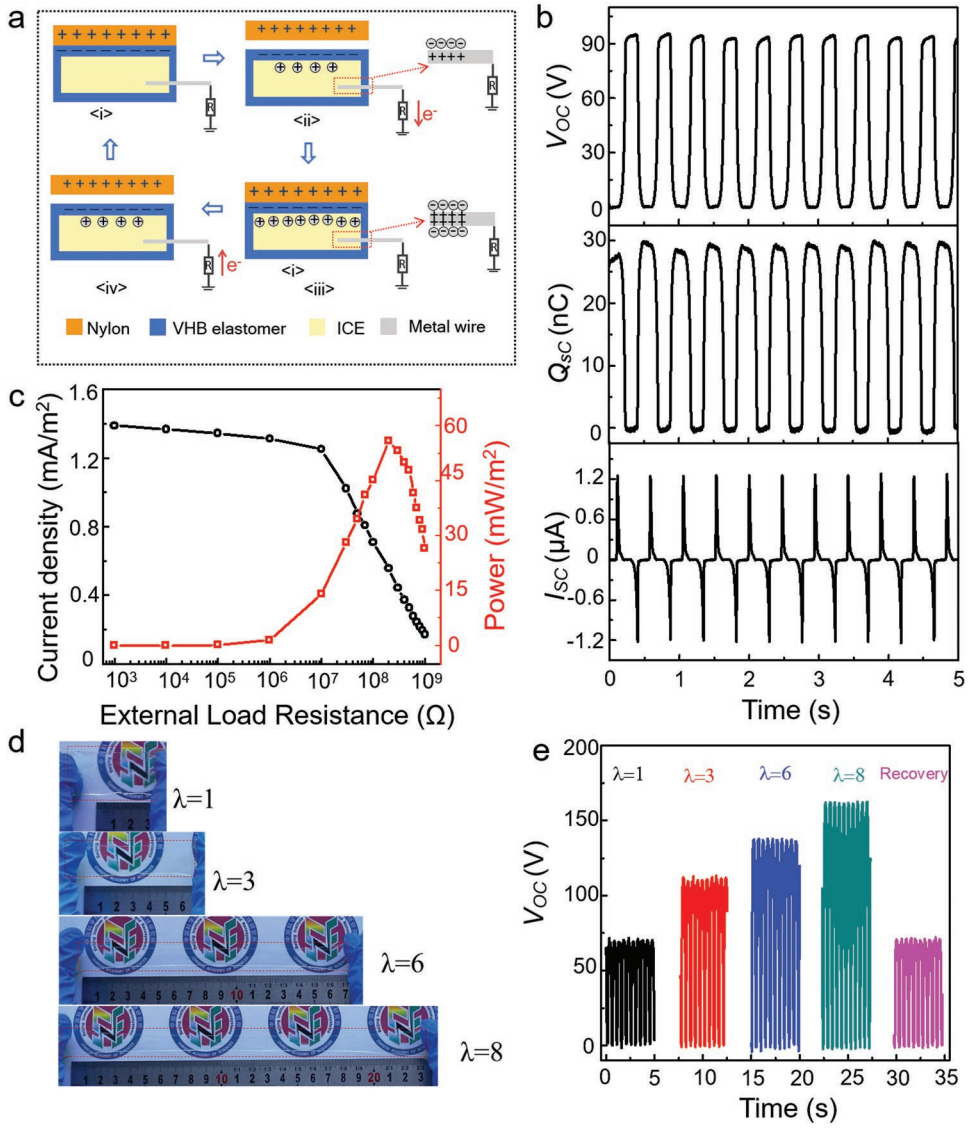

Figure 2. The working principles, output, and stretchability of the ICE-iTENG at single-electrode mode. a) Scheme of the working mechanism of the ICE-iTENG. b) Open-circuit voltage V_{OC}, short-circuit charge quantity Q_{SC}, and short-circuit current I_{SC} of an ICE-iTENG. c) Variation of the output current density and power density with the external loading resistance. d) Photos of the ICE-iTENG at initial state and different stretched states. e) The corresponding output V_{OC} when having contact-separation motion to a latex film.

When the iTENG was released from the stretched states, the values of V_{OC} and Q_{SC} were almost equal to the values at initial state. The results were similar with the results for PAAm-hydrogel iTENG at the stretched states.[46,49] For most stretchable devices with carbonaceous materials or metal nanowires conductive composites, the breakdown of conductive network at large strain always results in the degradation of electrical outputs. On the contrary, our devices with ICEs do not show any degradation. The electrical outputs are even improved at stretched states.

2.3. Environmental Stability of ICE-iTENG

Dehydration is almost inevitable for hydrogels. Even with a sealing layer, the evaporation of the water solvent at temperature above the boiling point still happens, which can possibly break or degrade the devices. After the dehydration, the shape, morphology, and mechanical and electrical properties were totally different from that at the fresh state.[44] On the contrary, ICEs were solvent-free, which eliminates the dehydration issue.

Figure 3a was the thermogravimetric curve of the ICE and PAAm hydrogel with 4 M LiCl in N_2 atmosphere. The weight of PAAm hydrogel continued to decrease with increasing temperature above 50 °C. However, the weight of the ICE was unchanged before 335 °C. Over 335 °C, the polymer chains started to decompose, showing a rapid weight decrease. It is obvious that the ICE is stable under 335 °C and possesses a wider working temperature range. Furthermore, the differential scanning calorimetry of ICE was measured. The result was shown in Figure S2 in the Supporting Information.

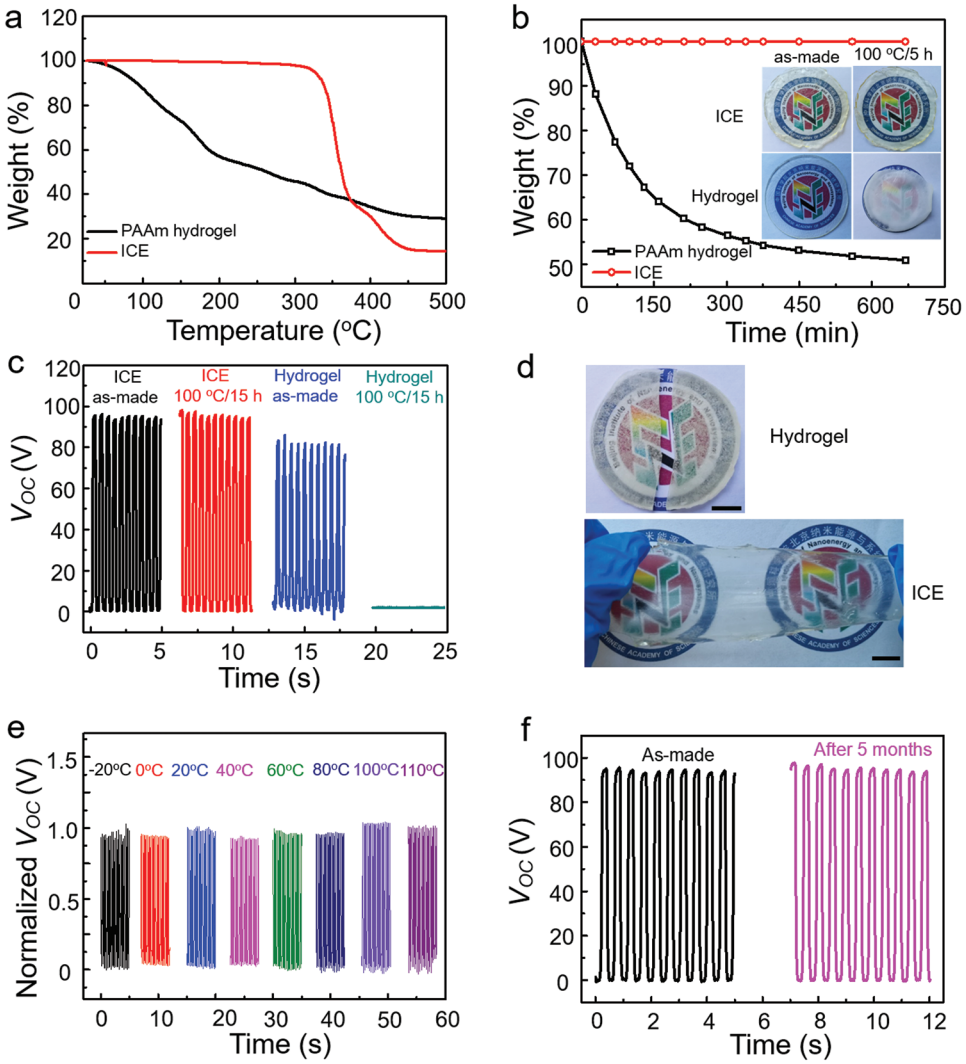

Figure 3. The durability of the ICE-iTENG. a) Thermogravimetric measurement of the ICE and PAAm-LiCl hydrogel. b) Weight retention of the hydrogel-iTENG and ICE-iTENG kept in an oven at 100 °C. The inset pictures were the ICE and PAAm hydrogel at as-made state and after being stored at 100 °C for 5 h. c) Comparison of the V_{OC} of the hydrogel-iTENG and ICE-iTENG at as-made state and after being stored at 100 °C for 15 h. d) The stretchability of the PAAm hydrogel and ICE being stored at 100 °C for 15 h (scale bar: 1 cm). e) Normalized V_{OC} value of an ICE-iTENG measured at different temperatures with contact-separation to a Nylon film (normalized to V_{OC} at 20 °C). f) Comparison of the V_{OC} of the ICE-iTENG before and after being stored at room temperature for 5 months.

The result shows that the glass-transition temperature (T_g) for ICE is around –40 °C. The molecular chain was cross-linked by PEGDA, so there was no obvious melting point for ICE before it starts thermal degradation (300 °C). The stability of PAAm hydrogel-iTENG and ICE-iTENG was compared at 100 °C in the oven. The weight was recorded over the time in Figure 3b. The results showed that the weight of ICE-iTENG remained unchanged at 100 °C during the experiment. However, the weight of PAAm-iTENG decreased to 57% drastically within 5 h at 100 °C. The decrease trend slowed after 5 h, and the weight remained 50% after 10 h. The inset pictures in Figure 3b were the ICE and PAAm hydrogel at as-made state and after being stored at 100 °C for 5 h. Comparing with the as-made state, there was no obvious change on the size and transparency for ICE after being stored for 5 h; while, the size of PAAm hydrogel reduced significantly and the sample became non-transparent due to the dehydration after being stored at 100 °C for 5 h. The pictures of the ICE and PAAm hydrogel being stored at 100 °C for 2 h and at room temperature in air for 5 months were shown in Figure S3 in the Supporting Information. There was no change neither in the size nor in the transparency for ICE after 5 months; whereas, the size of PAAm hydrogel reduced significantly and became non-transparent and fragile.

The ICE can attach to the metals strongly. The junction between the ICE and metal was even stable at stretch states. The strong adhesion property of ICE originated from the polymer substrate polybutylacrylate (PBA), a commonly used Acrylate Adhesive.[44] Photo demonstrating adhesive property of ICE was shown in Figure S4 in the Supporting Information.

The V_{OC} for the PAAm hydrogel-iTENG and ICE-iTENG before and after storing in an oven at 100 °C for 15 h were compared in Figure 3c. The peak V_{OC} was around 80 V for fresh

PAAm hydrogel-iTENG. When it was stored in an oven for 15 h at 100 °C, there was totally no output signal. The peak V_{OC} was around 92 V for fresh ICE-iTENG. When it was stored in an oven for 15 h at 100 °C, the V_{OC} almost remained the same. The stretchability of the PAAm hydrogel and ICE after being stored at 100 °C for 15 h was also studied in Figure 3d. The PAAm hydrogel dehydrated completely and became brittle when it was stored in an oven for 15 h at 100 °C. However, the ICE still possessed excellent stretchability. The stress-strain curves of the ICE before and after being stored at 100 °C for 15 h were shown in Figure S5 in the Supporting Information. The fracture strength for ICEs after being stored at 100 °C for 15 h is around 208 kPa and the strain to fracture is around 1000%., which are almost comparable to the as-made ICE,

The performances of the ICE-iTENG (area, 2×2 cm^2) at different temperatures (–20 to 110 °C) were tested. A Nylon film was used to carry out contact-separation movement. The Normalized V_{OC} was shown in Figure 3e and the Normalized Q_{SC} was shown in Figure S6 in the Supporting Information. From the results, the V_{OC} and Q_{SC} are quite stable at different temperatures. It indicated that the ICE-iTENG was quite stable at a wider high temperature range and had a great potential to be used in extreme environment.[46,48]

The durability of the ICE-iTENG over long-term motion cycles was also tested and the results were shown in Figure S7 in the Supporting Information. Repeating ≈5000 contact-separation motion cycles (for 1 h), the V_{OC} shows no obvious degradation. To confirm the durability of ICE-iTENG, the V_{OC} was test again after 5 months later. The results were shown in Figure 3f. There was no significant difference for V_{OC} between the fresh device and device kept in air for 5 months.

2.4. Hand-Tapping Energy Harvesting by the ICE-iTENG

The STENG can convert tiny mechanical energy in the environment into electrical energy.[40,51–55] In our experiment, we converted the energy of human motions into electrical energy by ICE-iTENG. When tapping an ICE-iTENG with one hand, the ICE-iTENG will work in the single-electrode mode. The human body can be treated as a reference electrode or grounding. The V_{OC}, Q_{SC}, I_{SC}, and rectified current an ICE-iTENG by hand-tapping is shown in Figure S8 in the Supporting Information. The output of an ICE-iTENG can be used to charge capacitors for powering various electronic devices. In demonstrative experiment, we use an ICE-iTENG to charge a 2.2-μF capacitor to power an electronic watch. The ICE-iTENG used to power the watch is in a circular shape and the diameter is 6 cm. The detailed photo and equivalent circuit of self-charging system was shown in **Figure 4**a,b, respectively. The capacitor was first charged by tapping the ICE-iTENG with one hand, and then the electronic watch was connected. The tapping frequency is around 4 Hz. The voltage of the 2.2-μF capacitor reached at 2.2 V in 60 s and then the electronic watch was powered for about 10 s (Figure 4c). The voltage of the capacitor decreased to 0.7 V. Subsequently, the capacitor was charged back to 2.2 V by tapping the ICE-iTENG again in around 40 s, and then the watch was powered repeatedly. In this case, the small electronics can be powered solely by the energy converted from the human motions. Each tapping motion can generate one pulsed output (Figure S8, Supporting Information), the electrical energy of which can be roughly estimated as $E = V_{oc}Q_{sc}$. Then, the total energy during the whole capacitor-charging process (4 Hz, 60 s) is calculated by $E_{iTENG} = \sum V_{oc}Q_{sc} = 4.8 \times 10^{-4}$ J (average V_{oc} and Q_{sc} is 80 V and 25 nC, obtained from Figure S8a,b, Supporting Information). The energy stored in 2.2-μF capacitor is calculated from the charging voltage profile by $E_{capacitor} = \frac{1}{2} C V^2 = 5.324 \times 10^{-6}$ J (C is 2.2 μF and V is 2.2 V). The average energy consumed by the watch is calculated by $E_{watch} = \frac{1}{2} C \Delta V^2 = 2.475 \times 10^{-6}$ J (ΔV is 1.5 V). The results show that $E_{iTENG}$is much larger than $E_{capacitor}$, suggesting a low energy utilization efficiency during the charging process due to the unmatched impedance between the ICE-iTENG and the capacitor.[56] For real application, power management has to be included to optimize the energy utilization efficiency.[57]

2.5. Tactile Sensing by the ICE-iTENG

Many efforts have been made to develop flexible triboelectric pressure sensors. For example, a hydrogel based iTENG flexible triboelectric sensor working in single-electrode-mode was reported.[46] The stretchability of the sensor is about 1000%; however, its pressure sensitivity is too low (0.013 kPa^{-1}) and can only responded to lager pressure (>1300 Pa). To achieve a sensor with high pressure sensitivity, we design a particular

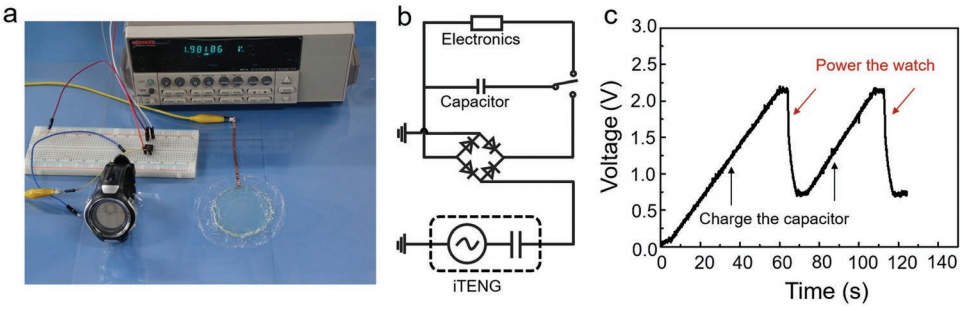

Figure 4. Biomechanical energy harvesting by the ICE-iTENG. a) A photo and b) the equivalent circuit of a self-charging system that uses the energy harvested from the ICE-iTENG to power electronics. c) Voltage profile of a 2.2-μF capacitor being charged by the ICE-iTENG and used to power the electronic watch.

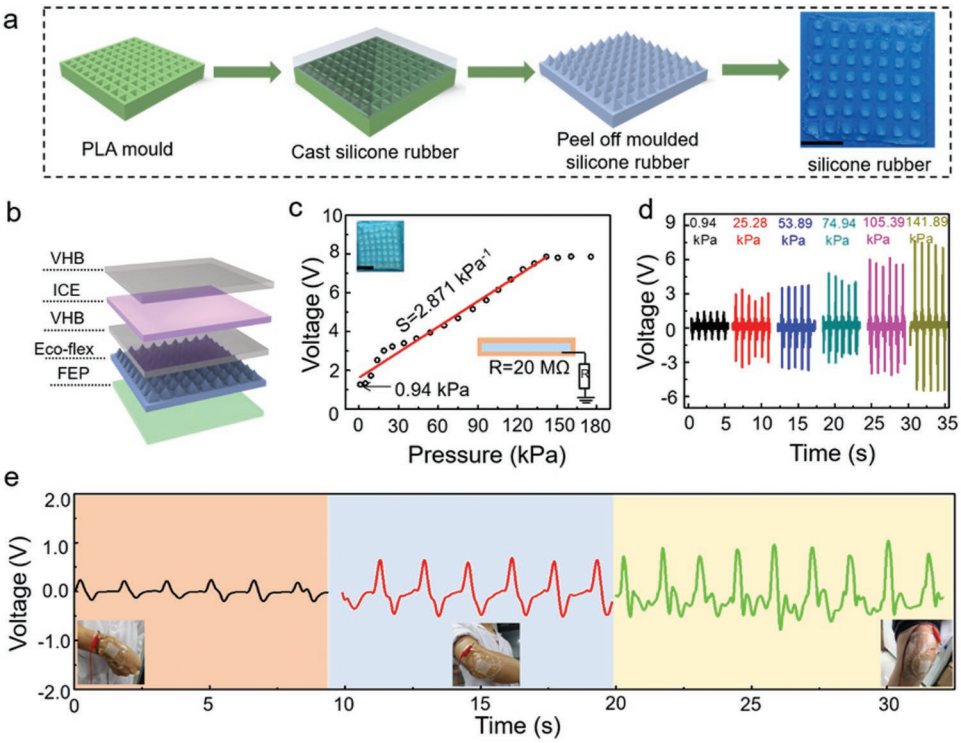

Figure 5. Pressure sensing by the ICE-iTENG. a) Schematic fabrication of Eco-flex with triangular prisms on surface (scale bar: 1 cm). b) Scheme of the ICE-iTENG sensor (scale bar: 1 cm). c) Summarized variation of peak amplitudes of the voltage with the contact pressure. Inset: photo of the ICE-iTENG tactile sensor (area, 3×3 cm^2). d) Representative voltage profiles of the ICE-iTENG as tactile sensor at six different pressures. e) Human activity monitoring with the ICE-iTENG pressure sensor.

structure for the sensor, as shown in **Figure 5**a. Eco-flex 00-20 silicone rubbers were used for the tribo-positive materials. Triangular pyramid structures were introduced onto Eco-flex rubber's surface as shown in Figure 5a. At first, a polylactic acid (PLA) mould with triangular pyramid groove was prepared by 3D printing machine. The height and width of the triangular pyramids are 1.86 and 2.46 mm, respectively. Then, the precursor of Eco-flex 00-20 was casted on the PLA mould and cured. In the end, an Eco-flex film with triangular pyramid features was peeled off from the mould. The sensor will work in the single-electrode mode as shown in Figure 5b. The fluorinated ethylene propylene (FEP) film was used to seal the Eco-flex silicone rubbers with the ICE-iTENG. The size of the tactile sensor was 3×3 cm^2 with a 3-mm thickness. The FEP serves as a cover of the sensor. The fresh-made Eco-flex 00-20 is slightly sticky, so we used FEP to avoid attach of Eco-flex to step motor during test. This film had no influence on the tactile sensor. The thickness of the Eco-flex layer is around 2.7 mm. When the pressure acting on the surface of sensor changed, different contact areas and deformation depth are formed due to the triangular pyramids, resulting in pressure-dependence outputs to external circuits. A 20-MΩ resistor was connected to the ICE-iTENG sensor (area, 3×3 cm^2), and the voltage drop across the resistor was recorded when pressing the sensor with different pressures (Figure 5c). The typical voltage output at different pressure was shown in Figure 5d. The amplitude of the bimodal voltage increases linearly with increasing the pressure when the touch pressure is low. It saturates when the pressure is higher than ≈140 kPa. The sensitivity (S) can be calculated as follows:

$$S = \left(d\Delta V / V_S\right)/dP \tag{3}$$

where ΔV denotes the relative change of the output voltage, V_S denotes the saturated voltage, and P denotes the touch pressure. The sensitivity of the ICE-iTENG sensor is calculated to be 2.87 kPa^{-1}, which is higher than many other sensors.[46,58,59] The sensor can detect pressure as low as 940 Pa. To output a voltage signal, there has to be a contact-separation motion between the VHB and Eco-flex. Better performances might be achieved by optimizing the materials choices of involved dielectric elastomers. Here, we mainly attempt to prove the concept of pressure sensing by using this structure. Bending the sensor can also result in the contact-separation of the patterned Eco-flex film and the VHB elastomer. Therefore, the ICE-iTENG pressure sensor can also be used to monitor the human activity. The output voltage of the sensor attached at different parts of the body (waist, elbow, and knee) was measured. Figure 5e illustrated the real-time voltage response when bending the waist, elbow, and knee, respectively. Each output signal was associated with the movement of the body (waist, elbow, and knee). Comparing with the voltage obtained from waist bending, the voltages from elbow and knee bending are larger, indicating the larger strain of the ICE-iTENG.

3. Conclusion

In summary, a new iTENG based on an ICE was designed. The resultant ICE-iTENG showed high transparency, high stretchability, and stable electrical performance over a wide temperature range from −20 to 110 °C. The dehydration or evaporation of liquid solvent is completely avoided for this ICE-iTENG, and the ICE is thermally stable until about 335 °C. Even after hours of storing at 100 °C, the ICE-iTENG shows no degradation in the electrical performances, which is highly desirable for a next-generation stretchable power source. We demonstrated effective biomechanical energy harvesting by the ICE-iTENG, indicating its great potential for applications in self-powered electronics. Furthermore, a transparent pressure sensor with high sensitivity was achieved by constructing triangular pyramid structures on the surface of triboelectric material. The sensitivity of the ICE-iTENG sensor is 2.871 kPa^{-1}, and the detection pressure limit is as low as 940 Pa.

4. Experimental Section

Fabrication of ICEs: ICEs were fabricated by photopolymerization. LiTFSI was used as the electrolyte salt, and BA, PEGDA, 1-hydroxycyclohexyl phenyl ketone (photo-initiator 184) were used as monomer, crosslinker, and photo-initiator, respectively (Figure 1a). The detailed preparation of ICEs is as follows: at first, LiTFSI, PEGDA, and photo-initiator 184 were dissolved in BA. The molar percentage of PEGDA and photo-initiator 184 to BA were 0.1% and 1% throughout the entire experiments, respectively. The molar concentration of LiTFSI was fixed at 0.5 M. Then, the solution was injected into a polytetrafluoroethylene mold. In the end, an UV light irradiation (365 nm, 400 W power) was adopted to initiate the polymerization.

Fabrication of the PAAm-LiCl Hydrogel: At first, acrylamide was added into 4 M LiCl aqueous solution. The weight concentration of acrylamide relative to deionized water was 14%. Subsequently, N,N′-methylenebisacrylamide, ammonium persulfate, and N,N,N′,N′-tetramethylethylenediamine were dissolved in the solution consecutively. The solution was then transferred into a glass mold and treated in an oven at 50 °C for 2 h to form the PAAm-LiCl hydrogel. The thickness of the final hydrogel was controlled by the volume of the solution and is around 2 mm.

Fabrication of the iTENGs: The VHB film (thickness is 130 µm, 3 M VHB 9469) was used as electrification layer elastomer. The PAAm-LiCl hydrogel, ICEs, and VHB were cut into the desired shape with a laser cutter. The final device was fabricated by wrapping and sealing the PAAm-LiCl hydrogel or ICEs with the VHB films. A Cu wire was attached to the hydrogel or ICEs for electrical connection.

Characterization and Measurements: A step motor (LinMot E1100) was used to provide the input of mechanical motions. For all the tests of energy generation of the iTENG, the pressure (100 kPa), speed (2 m s^{-1}), and frequency (≈2 Hz) of the step motor were fixed. The voltage and charge quantity were recorded by a Keithley electrometer 6514, and the current was recorded with a Stanford low-noise preamplifier SR570. The force applied by the motor was detected by a Mark-10 force gauge. The mechanical tensile test and stretch cycling test of the iTENGs were conducted by an ESM301/Mark-10 system. For the tensile test, the strain rate was fixed at 30 mm min^{-1}. For the measurement of the output performances of the iTENG at different temperatures, the iTENG was kept inside a thermostat oven (GDW-50L, Wuxi Zhongtian Company), and the contact-separation motion was controlled by the linear motor outside through a feed through hole. The optical transmittance was measured by a Shimadzu UV-3600 spectrophotometer. Informed signed consent was obtained from the volunteer for the hand-tapping and tactile sensing tests.

Supporting Information

Supporting Information is available from the Wiley Online Library or from the author.

Acknowledgements

The authors thank for the support from National Key Research and Development Program of China (2016YFA0202703), National Natural Science Foundation of China (grant no. 51603013), the Youth Innovation Promotion Association of CAS, and Youth Backbone Individual Project Supported by Beijing Excellent Talents Training.

Conflict of Interest

The authors declare no conflict of interest.

Keywords

ion-conducting elastomers, pressure sensor, stretchable, transparent, triboelectric nanogenerators

Received: November 6, 2019
Revised: December 19, 2019
Published online: February 21, 2020

[1] B. Tian, T. Cohen-Karni, Q. Qing, X. Duan, P. Xie, C. M. Lieber, *Science* **2010**, *329*, 830.
[2] T. Sekitani, U. Zschieschang, H. Klauk, T. Someya, *Nat. Mater.* **2010**, *9*, 1015.
[3] Y.-C. Lai, H.-M. Wu, H.-C. Lin, C.-L. Chang, H.-H. Chou, Y.-C. Hsiao, Y.-C. Wu, *Adv. Funct. Mater.* **2019**, *29*, 1904626.
[4] C. Larson, B. Peele, S. Li, S. Robinson, M. Totaro, L. Beccai, B. Mazzolai, R. Shepherd, *Science* **2016**, *351*, 1071.
[5] K. Parida, G. Thangavel, G. Cai, X. Zhou, S. Park, J. Xiong, P. S. Lee, *Nat. Commun.* **2019**, *10*, 2158.
[6] S. Park, G. Thangavel, K. Parida, S. Li, P. S. Lee, *Adv. Mater.* **2019**, *31*, 1805536.
[7] R. Hinchet, W. Seung, S.-W. Kim, *ChemSusChem* **2015**, *8*, 2327.
[8] H. Wu, Y. Huang, F. Xu, Y. Duan, Z. Yin, *Adv. Mater.* **2016**, *28*, 9881.
[9] F. R. Fan, W. Tang, Z. L. Wang, *Adv. Mater.* **2016**, *28*, 4283.
[10] F.-R. Fan, Z.-Q. Tian, Z. L. Wang, *Nano Energy* **2012**, *1*, 328.
[11] J. W. Lee, S. Jung, T. W. Lee, J. Jo, H. Y. Chae, K. Choi, J. J. Kim, J. H. Lee, C. Yang, J. M. Baik, *Adv. Energy Mater.* **2019**, *9*, 1901987.
[12] J. P. Lee, J. W. Lee, B.-K. Yoon, H. J. Hwang, S. Jung, K. A. Kim, D. Choi, C. Yang, J. M. Baik, *Nano Energy* **2019**, *56*, 571.
[13] T. Kumari, S. Jung, Y. Cho, H.-P. Kim, J. W. Lee, J. Oh, J. Lee, S. M. Lee, M. Jeong, J. M. Baik, W. Jo, C. Yang, *Nano Energy* **2020**, *68*, 104327.
[14] Y.-C. Lai, J. Deng, S. Niu, W. Peng, C. Wu, R. Liu, Z. Wen, Z. L. Wang, *Adv. Mater.* **2016**, *28*, 10024.
[15] F. Yi, J. Wang, X. Wang, S. Niu, S. Li, Q. Liao, Y. Xu, Z. You, Y. Zhang, Z. L. Wang, *ACS Nano* **2016**, *10*, 6519.
[16] F. Yi, L. Lin, S. Niu, P. K. Yang, Z. Wang, J. Chen, Y. Zhou, Y. Zi, J. Wang, Q. Liao, Y. Zhang, Z. L. Wang, *Adv. Funct. Mater.* **2015**, *25*, 3688.
[17] B.-U. Hwang, J.-H. Lee, T. Tran Quang, E. Roh, D.-I. Kim, S.-W. Kim, N.-E. Lee, *ACS Nano* **2015**, *9*, 8801.
[18] K. N. Kim, J. Chun, J. W. Kim, K. Y. Lee, J.-U. Park, S.-W. Kim, Z. L. Wang, J. M. Baik, *ACS Nano* **2015**, *9*, 6394.

[19] X. Chen, X. Pu, T. Jiang, A. Yu, L. Xu, Z. L. Wang, *Adv. Funct. Mater.* **2017**, *27*, 1603788.
[20] P. J. Taroni, G. Santagiuliana, K. Wan, P. Calado, M. Qiu, H. Zhang, N. M. Pugno, M. Palma, N. Stingelin-Stutzman, M. Heeney, O. Fenwick, M. Baxendale, E. Bilotti, *Adv. Funct. Mater.* **2018**, *28*, 1704285.
[21] F. Yi, X. Wang, S. Niu, S. Li, Y. Yin, K. Dai, G. Zhang, L. Lin, Z. Wen, H. Guo, J. Wang, M.-H. Yeh, Y. Zi, Q. Liao, Z. You, Y. Zhang, Z. L. Wang, *Sci. Adv.* **2016**, *2*, e1501624.
[22] X. Pu, M. Liu, X. Chen, J. Sun, C. Du, Y. Zhang, J. Zhai, W. Hu, Z. L. Wang, *Sci. Adv.* **2017**, *3*, e1700015.
[23] L. Sun, S. Chen, Y. Guo, J. Song, L. Zhang, L. Xiao, Q. Guan, Z. You, *Nano Energy* **2019**, *63*, 103847.
[24] K. Parida, V. Kumar, J. Wang, V. Bhavanasi, R. Bendi, P. S. Lee, *Adv. Mater.* **2017**, *29*, 1702181.
[25] H. J. Hwang, J. S. Kim, W. Kim, H. Park, D. Bhatia, E. Jee, Y. S. Chung, D. H. Kim, D. Choi, *Adv. Energy Mater.* **2019**, *9*, 1803786.
[26] G. Zhao, Y. Zhang, N. Shi, Z. Liu, X. Zhang, M. Wu, C. Pan, H. Liu, L. Li, Z. L. Wang, *Nano Energy* **2019**, *59*, 302.
[27] Y. Ding, J. Zhang, L. Chang, X. Zhang, H. Liu, L. Jiang, *Adv. Mater.* **2017**, *29*, 1704253.
[28] Y. Lee, S. H. Cha, Y.-W. Kim, D. Choi, J.-Y. Sun, *Nat. Commun.* **2018**, *9*, 1804.
[29] L. M. Zhang, Y. He, S. Cheng, H. Sheng, K. Dai, W. J. Zheng, M. X. Wang, Z. S. Chen, Y. M. Chen, Z. Suo, *Small* **2019**, *15*, 1804651.
[30] C. Yang, Z. Suo, *Nat. Rev. Mater.* **2018**, *3*, 125.
[31] J.-Y. Sun, C. Keplinger, G. M. Whitesides, Z. Suo, *Adv. Mater.* **2014**, *26*, 7608.
[32] Q. Guan, G. Lin, Y. Gong, J. Wang, W. Tan, D. Bao, Y. Liu, Z. You, X. Sun, Z. Wen, Y. Pan, *J. Mater. Chem. A* **2019**, *7*, 13948.
[33] W. Xu, L.-B. Huang, M.-C. Wong, L. Chen, G. Bai, J. Hao, *Adv. Energy Mater.* **2017**, *7*, 1601529.
[34] T. Liu, M. Liu, S. Dou, J. Sun, Z. Cong, C. Jiang, C. Du, X. Pu, W. Hu, Z. L. Wang, *ACS Nano* **2018**, *12*, 2818.
[35] J.-Y. Sun, X. Zhao, W. R. K. Illeperuma, O. Chaudhuri, K. H. Oh, D. J. Mooney, J. J. Vlassak, Z. Suo, *Nature* **2012**, *489*, 133.
[36] H. Liu, Y. Wang, K. Cui, Y. Guo, X. Zhang, J. Qin, *Adv. Mater.* **2019**, *31*, 1902042.
[37] X. P. Morelle, W. R. Illeperuma, K. Tian, R. Bai, Z. Suo, J. J. Vlassak, *Adv. Mater.* **2018**, *30*, 1801541.
[38] P. Calvert, *Adv. Mater.* **2009**, *21*, 743.
[39] B. Chen, W. Tang, T. Jiang, L. Zhu, X. Chen, C. He, L. Xu, H. Guo, P. Lin, D. Li, J. Shao, Z. L. Wang, *Nano Energy* **2018**, *45*, 380.
[40] Z. L. Wang, *ACS Nano* **2013**, *7*, 9533.
[41] G. Ge, Y. Zhang, J. Shao, W. Wang, W. Si, W. Huang, X. Dong, *Adv. Funct. Mater.* **2018**, *28*, 1802576.
[42] W. H. Meyer, *Adv. Mater.* **1998**, *10*, 439.
[43] Z. Xue, D. He, X. Xie, *J. Mater. Chem. A* **2015**, *3*, 19218.
[44] L. Shi, T. Zhu, G. Gao, X. Zhang, W. Wei, W. Liu, S. Ding, *Nat. Commun.* **2018**, *9*, 2630.
[45] Y. Kitazawa, K. Iwata, R. Kido, S. Imaizumi, S. Tsuzuki, W. Shinoda, K. Ueno, T. Mandai, H. Kokubo, K. Dokko, M. Watanabe, *Chem. Mater.* **2018**, *30*, 252.
[46] X. Pu, M. Liu, X. Chen, J. Sun, C. Du, Y. Zhang, J. Zhai, W. Hu, Z. L. Wang, *Sci. Adv.* **2017**, *3*, e1700015.
[47] C. Keplinger, J.-Y. Sun, C. C. Foo, P. Rothemund, G. M. Whitesides, Z. Suo, *Science* **2013**, *341*, 984.
[48] X. Wen, Y. Su, Y. Yang, H. Zhang, Z. L. Wang, *Nano Energy* **2014**, *4*, 150.
[49] S. M. Niu, Z. L. Wang, *Nano Energy* **2015**, *14*, 161.
[50] S. Niu, Y. Liu, S. Wang, L. Lin, Y. S. Zhou, Y. Hu, Z. L. Wang, *Adv. Funct. Mater.* **2014**, *24*, 3332.
[51] Z. L. Wang, *Nature* **2017**, *542*, 159.
[52] Y.-C. Lai, J. Deng, R. Liu, Y.-C. Hsiao, S. L. Zhang, W. Peng, H.-M. Wu, X. Wang, Z. L. Wang, *Adv. Mater.* **2018**, *30*, 1801114.
[53] X. Pu, L. Li, M. Liu, C. Jiang, C. Du, Z. Zhao, W. Hu, Z. L. Wang, *Adv. Mater.* **2016**, *28*, 98.
[54] Y. Yu, H. Sun, H. Orbay, F. Chen, C. G. England, W. Cai, X. Wang, *Nano Energy* **2016**, *27*, 275.
[55] X. Pu, W. Song, M. Liu, C. Sun, C. Du, C. Jiang, X. Huang, D. Zou, W. Hu, Z. L. Wang, *Adv. Energy Mater.* **2016**, *6*, 1601048.
[56] X. Pu, M. Liu, L. Li, C. Zhang, Y. Pang, C. Jiang, L. Shao, W. Hu, Z. L. Wang, *Adv. Sci.* **2016**, *3*, 1500255.
[57] F. Xi, Y. Pang, W. Li, T. Jiang, L. Zhang, T. Guo, G. Liu, C. Zhang, Z. L. Wang, *Nano Energy* **2017**, *37*, 168.
[58] X. Wang, H. Zhang, L. Dong, X. Han, W. Du, J. Zhai, C. Pan, Z. L. Wang, *Adv. Mater.* **2016**, *28*, 2896.
[59] L. Pan, A. Chortos, G. Yu, Y. Wang, S. Isaacson, R. Allen, Y. Shi, R. Dauskardt, Z. Bao, *Nat. Commun.* **2014**, *5*, 3002.